

# Structure-Guided Optimization of Inhibitors of Acetyltransferase Eis from *Mycobacterium tuberculosis*

Ankita Punetha,<sup>1</sup> Huy X. Ngo,<sup>1</sup> Selina Y. L. Holbrook, Keith D. Green, Melisa J. Willby, Shilah A. Bonnett, Kyle Krieger, Emily K. Dennis, James E. Posey, Tanya Parish, Oleg V. Tsodikov,\* and Sylvie Garneau-Tsodikova\*



Cite This: <https://dx.doi.org/10.1021/acscchembio.0c00184>



Read Online

ACCESS |



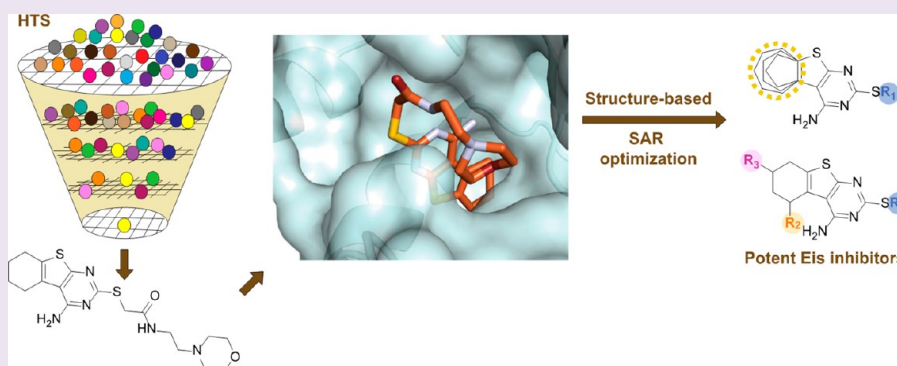
Metrics & More



Article Recommendations



Supporting Information



**ABSTRACT:** The enhanced intracellular survival (Eis) protein of *Mycobacterium tuberculosis* (*Mtb*) is a versatile acetyltransferase that multiacetylates aminoglycoside antibiotics abolishing their binding to the bacterial ribosome. When overexpressed as a result of promoter mutations, Eis causes drug resistance. In an attempt to overcome the Eis-mediated kanamycin resistance of *Mtb*, we designed and optimized structurally unique thieno[2,3-*d*]pyrimidine Eis inhibitors toward effective kanamycin adjuvant combination therapy. We obtained 12 crystal structures of enzyme–inhibitor complexes, which guided our rational structure-based design of 72 thieno[2,3-*d*]pyrimidine analogues divided into three families. We evaluated the potency of these inhibitors *in vitro* as well as their ability to restore the activity of kanamycin in a resistant strain of *Mtb*, in which Eis was upregulated. Furthermore, we evaluated the metabolic stability of 11 compounds *in vitro*. This study showcases how structural information can guide Eis inhibitor design.

## INTRODUCTION

The advent of antibiotics, including antitubercular agents, has been one of the most powerful technological advances responsible for the reduction of mortality due to bacterial infections.<sup>1</sup> Unfortunately, in the last few decades, due to the overuse and misuse of the same antibiotics and the paucity of new antibacterial agents, resistance to antibiotics has emerged as a global crisis. There is a pressing need for discovery of new molecules and strategies to combat antibiotic resistance. In 2018, tuberculosis (TB), caused by infections with *Mycobacterium tuberculosis* (*Mtb*), killed 1.5 million people, which is more than any other infection worldwide, and caused 10 million new cases.<sup>2</sup> Misuse of anti-TB drugs, poor treatment compliance, and over 50 years of using many of the same antibiotics to fight this disease have led to the emergence and spread of *Mtb* strains resistant to one or more of these agents. Multidrug-resistant (MDR) *Mtb* strains that cause MDR TB are, by definition, resistant to first-line drugs isoniazid and rifampin, taken orally. A second-line antibiotic, aminoglycoside kanamycin (KAN) is used to treat MDR TB, but resistance to

KAN, a hallmark of extensively drug-resistant (XDR) TB (along with resistance to a fluoroquinolone), has also emerged and spread. XDR TB has a high mortality rate and requires prolonged treatment that can last as long as 2 years, even if successful. A clinically significant mechanism of KAN resistance in TB is KAN acetylation by the acetyltransferase Eis as a result of point mutations in the *eis* promoter or the 5' untranslated region of the gene encoding a transcription factor WhiB7.<sup>3–5</sup>

We previously showed that Eis transfers an acetyl group from acetyl coenzyme A (AcCoA) to one or more amino groups of all clinically relevant aminoglycosides,<sup>6–10</sup> abolishing their antibacterial activity. In addition, Eis can acetylate the

Received: March 12, 2020

Accepted: May 4, 2020



peptide antibiotic capreomycin.<sup>11</sup> This versatility is apparently enabled by a large substrate binding site that is lined largely by acidic and hydrophobic residues.<sup>6,8,12</sup> The acetylation reaction proceeds via a random sequential mechanism, where either AcCoA or the aminoglycoside substrate can bind first to a free enzyme.<sup>13</sup>

Two orthogonal approaches to overcoming Eis-mediated aminoglycoside resistance have been considered: (1) chemical modifications of existing aminoglycosides or development of novel aminoglycosides that would not succumb to acetylation by Eis, and (2) development of Eis inhibitors as adjuvants of the clinically used aminoglycosides. The first approach has been used successfully to design  $\beta$ -lactam antibiotics that are not susceptible to inactivation by  $\beta$ -lactamases.<sup>14</sup> Because of the very broad substrate versatility of Eis, an analogous approach of developing aminoglycosides that would not be susceptible to acetylation by Eis does not appear to be promising. Instead, our groups have focused on development of potent small molecule Eis inhibitors for their therapeutic use as aminoglycoside adjuvants against MDR TB.<sup>15–21</sup> We have discovered by high-throughput screening (HTS) Eis inhibitors of several structural families. Optimization of these molecules by classical medicinal chemistry has yielded several compounds that displayed potency (nanomolar in some cases) in inhibiting Eis in the test tube and in overcoming KAN resistance of a relevant resistant *Mtb* strain in culture.<sup>15–20</sup> In these studies, the crystal structures of Eis in complexes with several of these inhibitors showed that these inhibitors occupied the aminoglycoside binding site, in agreement with steady-state kinetic studies. These structures also established the molecular basis behind the inhibitor specificity and explained the structure–activity relationships (SAR).

In the current study, we report the discovery of Eis inhibitors with a chemical scaffold that is distinct from the previously reported ones. Here, crystal structures of Eis–inhibitor complexes are used to guide synthetic efforts in generating derivatives for further preclinical testing.

## RESULTS AND DISCUSSION

**Thieno[2,3-*d*]pyrimidine-Containing Eis Inhibitor.** To identify potential *Mtb* Eis inhibitors, HTS of ~23 000 structurally diverse compounds was carried out using our previously established aminoglycoside acetylation assay with *Mtb* Eis (Figure 1; step 1).<sup>15</sup> The HTS assay had a Z' score<sup>22</sup> of 0.65, indicating its robustness. Among the ~23 000 molecules tested, compound **2i** containing a thieno[2,3-*d*]pyrimidine moiety was an HTS hit ( $Z = 4.9$ , Figure 1; step 2). Eis inhibitors with this structural core have not been characterized previously.

In order to validate **2i** as an Eis inhibitor, we measured the dose response of the acetylation in the same assay (Figure 1, step 3) using a purchased fresh powder of **2i**. We then resynthesized **2i** and all analogues (Figure 1, step 4; characterization of all analogues in this study is shown in Figures S1–S222). We observed robust inhibition of Eis in this dose–response experiment, with an  $IC_{50}$  of  $1.6 \pm 0.2 \mu\text{M}$ . To test and validate the mechanism of action of **2i** as an Eis inhibitor in the *Mtb* cell, we determined the effect of **2i** on the MIC of KAN for the model strain *Mtb* K204, which bears a single clinically relevant mutation in the *eis* promoter resulting in Eis overexpression and KAN resistance<sup>3</sup> ( $MIC_{KAN}$  in K204 is  $>10 \mu\text{g/mL}$ ) in the background of strain H37Rv ( $MIC_{KAN} = 1.25 \mu\text{g/mL}$ ). *Mtb* K204 was used extensively to observe the

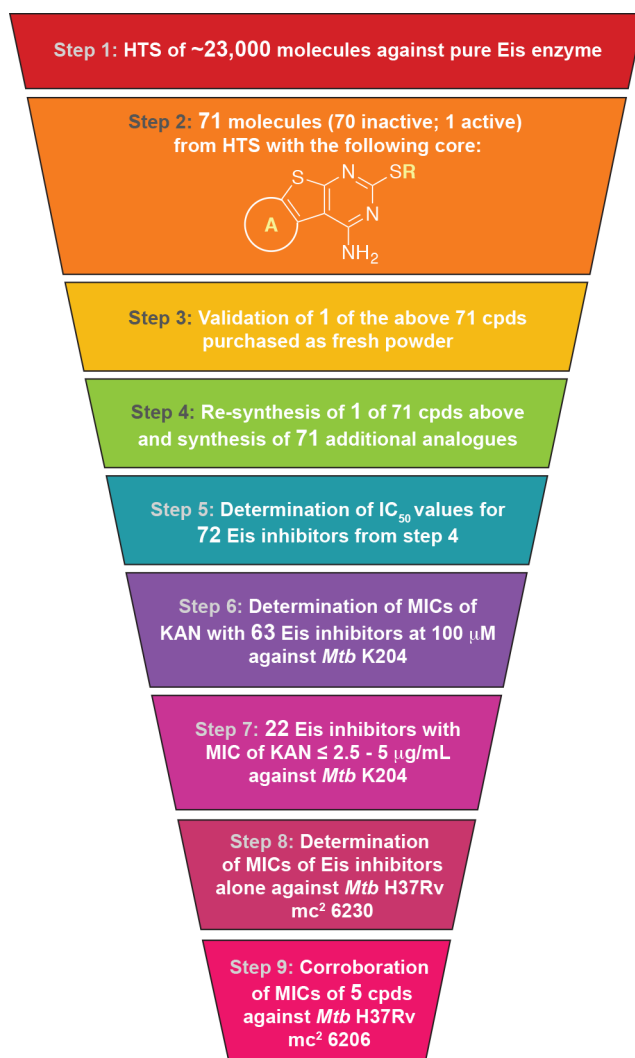


**Figure 1.** Cone diagram showing the evaluation and triage of ~23 000 structurally diverse compounds.

effect of our previously reported Eis inhibitors.<sup>16–20</sup> We observed that when tested at  $100 \mu\text{M}$ , **2i** restored, within a 2-fold dilution, the sensitivity of *Mtb* K204 to KAN to the level of the parent strain H37Rv ( $MIC_{KAN} = 2.5 \mu\text{g/mL}$  against *Mtb* K204 in the presence of **2i**).

**Structural Basis for Lead Compound Binding and Analogue Design.** The HTS library contained 70 other molecules with a thieno[2,3-*d*]pyrimidine moiety, which were not identified as hits (Figure S223). These inactive compounds aided our analogue design by demonstrating what chemical modifications to avoid (e.g., aromatic groups in the thioether side chain; heteroatoms in ring A; or substituents on the primary amine of ring C; see Figure 2 for ring labeling). To guide our inhibitor design, we determined a crystal structure of *Mtb* Eis in a complex with lead inhibitor **2i** (Figure 2A,B; PDB ID 6VUT; Table S1). As a reference structure, we chose the crystal structure of Eis in complex with inhibitor **39b** from a previous study (Figure 2C; PDB ID 6B3T).<sup>20</sup> Inhibitor **39b** contains a 1,2,4-triazino[5,6*b*]indole-3-thioether core that is partially isosteric with the tricyclic moiety of **2i**. Both **2i** and **39b** contain flexible substituents on the same side of the tricyclic moieties, each on a nitrogen-containing ring. Similar to **39b** and all the other previously reported inhibitors, **2i** is

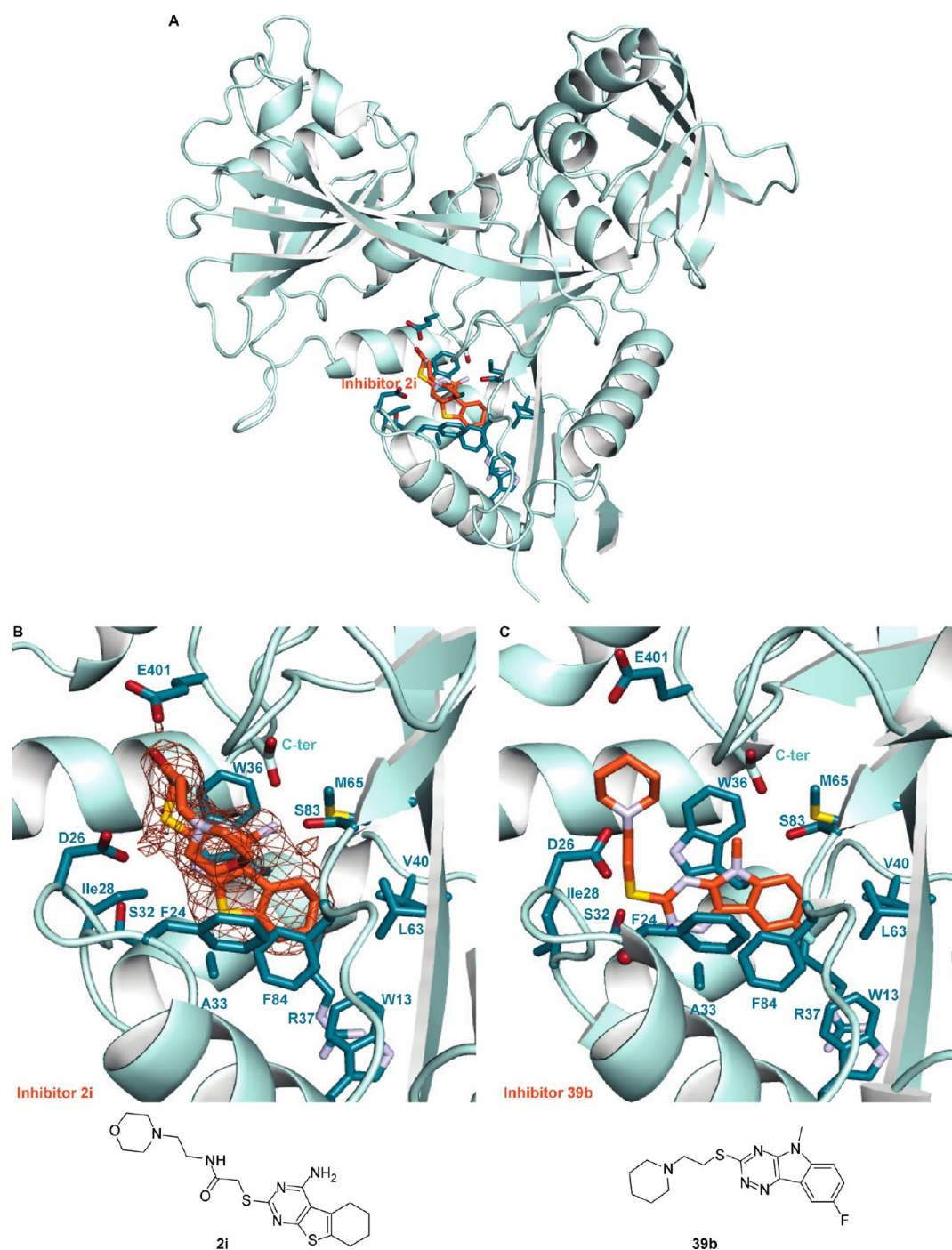


**Figure 2.** Crystal structures of Eis (one monomer is shown) in complex with inhibitors. (A) Crystal structure of Eis–2i complex. Eis is shown in cyan and 2i as orange sticks. (B) Zoomed-in view of the Eis–2i interface. The polder omit map for the inhibitor is contoured at  $4\sigma$  and is shown by the brown mesh. The amino acid residues interacting with compound 2i are shown by dark turquoise sticks. The nitrogen atoms are in light blue, oxygen atoms in red, sulfur atoms in yellow, and fluorine atoms in cyan. The C-terminus is labeled “C-ter”. (C) Previously reported crystal structure of Eis–39b complex (PDB ID 6B3T).<sup>20</sup> A water molecule in the active site is shown as a red sphere. The chemical structures of the bound inhibitors are shown on the bottom of panels B and C. Note: This color scheme is preserved in all the other figures depicting crystal structures.

bound in the aminoglycoside binding pocket (Figure S224). Strikingly, despite their similar shapes, the tricyclic moieties of 2i and 39b lie in the same plane, sandwiched between Trp36 and Phe84 but in different orientations that are related by a  $180^\circ$  rotation around an axis lying in the plane of these moieties and passing through the three rings. This difference, nevertheless, preserves the common binding characteristic, where the entirely hydrophobic ring A that is unsubstituted (in

2i) or modified by small nonpolar or weakly polar substitutions (a fluorine in 39b) abuts the hydrophobic wall of the binding pocket (lined with Trp13, the aliphatic portion of Arg37, Val40, Leu63, and Met65), whereas the large ( $R_1$ ) substituent on the opposite ring C is extended along the substrate binding cleft toward the solvent, a general direction of the thioether side chain. We used these properties of rings A and C and their substituents in our analogue design (Figure 3).

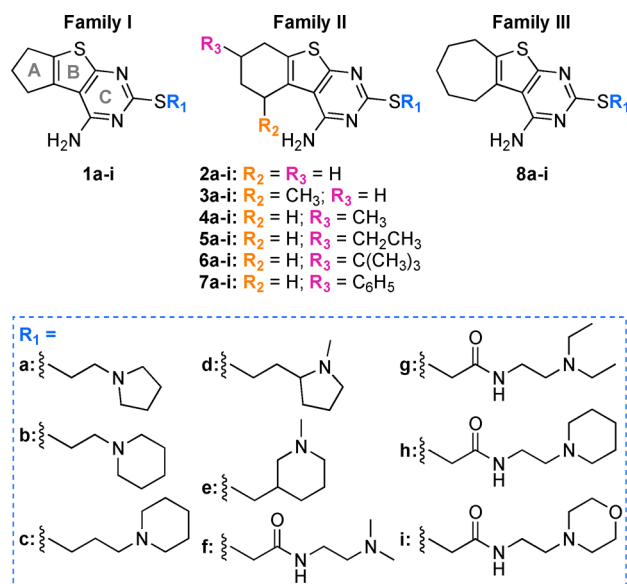


**Figure 3.** Chemical structures of all compounds synthesized and investigated in this study. The three rings of the tricyclic inhibitors in the library are labeled as A, B, and C for simplicity. The library is divided into three families (I–III) based on the size of ring A. Further subdivision of the families is based on  $R_1$ ,  $R_2$ , and  $R_3$  substituents.

Since relatively small hydrophobic substitutions on ring A were allowed, consistent with its environment, we varied the size of this ring and the presence and the nature of small hydrophobic substituents  $R_2$  and  $R_3$  at two positions on this ring. The difference in the orientations indicates that the specific chemical structures of the rings and their substitutions specify how the inhibitors are bound to the enzyme. Indeed, ring C in the thieno[2,3-*d*]pyrimidine core of **2i** is decorated with a primary amino group, absent in **39b**, which forms a salt bridge with the C-terminal carboxyl group of Eis. The primary amine on ring C is also preserved in all analogues, as it defines the overall disposition of the core of these the thieno[2,3-*d*]pyrimidines in the Eis binding pocket. There is not enough room to accommodate substitutions on this amino group, which explains inactivity of library compounds with such substitutions (Figure S223). The nonpolar sulfur of the central ring B of **2i** is in favorable hydrophobic contact with the side chain of Ala33 (the  $C_\beta$ –S distance is 3.6 Å), whereas the orientation of **39b** places its nitrogen-containing ring C approximately in the same site as the sulfur of **2i** but somewhat closer to the protein surface, enabling water-mediated hydrogen bonding of this ring with the amide nitrogens of Ile28 and Gly29. The sulfur-containing ring B is preserved in the analogues to maintain the interactions of this ring with Eis. For **2i**, a water mediates hydrogen bonding of a nitrogen of ring C with the side chain of Asp26. In both structures, the  $R_1$  is a thioether-linked side chain on ring C. In **2i**,  $R_1$  contains an additional amide ultimately connecting to a terminal morpholine ring, whereas in **39b**  $R_1$  is shorter and is terminated by a piperidine ring on an entirely hydrophobic linker. As a result of the different core orientations, the directions and interactions with the protein of  $R_1$  linkers (i.e., what links the sulfur atom and the tertiary amine of the thioether side chain) are somewhat different for **2i** and **39b**. While in **39b** the  $R_1$  linker is directed to sterically contact the backbone of Phe27–Asp26, the  $R_1$  of **2i** is directed along the other side of the binding cleft, in steric contact with the

backbone and the side chain of Glu401. For both **39b** and **2i**, the tertiary amines of  $R_1$  formed a salt bridge with Asp26, which for **2i** is enabled by its longer linker assuming a U-turn conformation. The position and the overall dimensions of the substituent on ring C, as a thin linker fitting the narrow Eis cleft, were also preserved in the analogues, whereas the nature of the substituents was different. An Eis loop spanning residues 25–30 is in two somewhat different conformations in the two structures, apparently induced by binding of the two different inhibitors. Most significantly, rotamers of Ile28 and Asp26 differ considerably in the two structures to optimally interact with the  $R_1$  linker and the terminal  $R_1$  group, respectively. The side chain of Arg37 is also in two different conformations, interacting with either the unmodified ring A of **2i** or with the fluorinated ring A of **39b**.

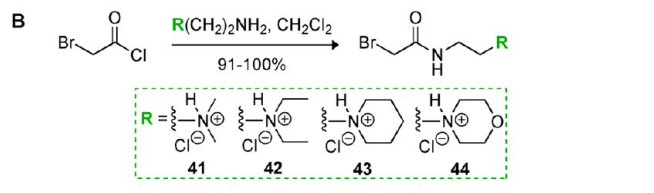
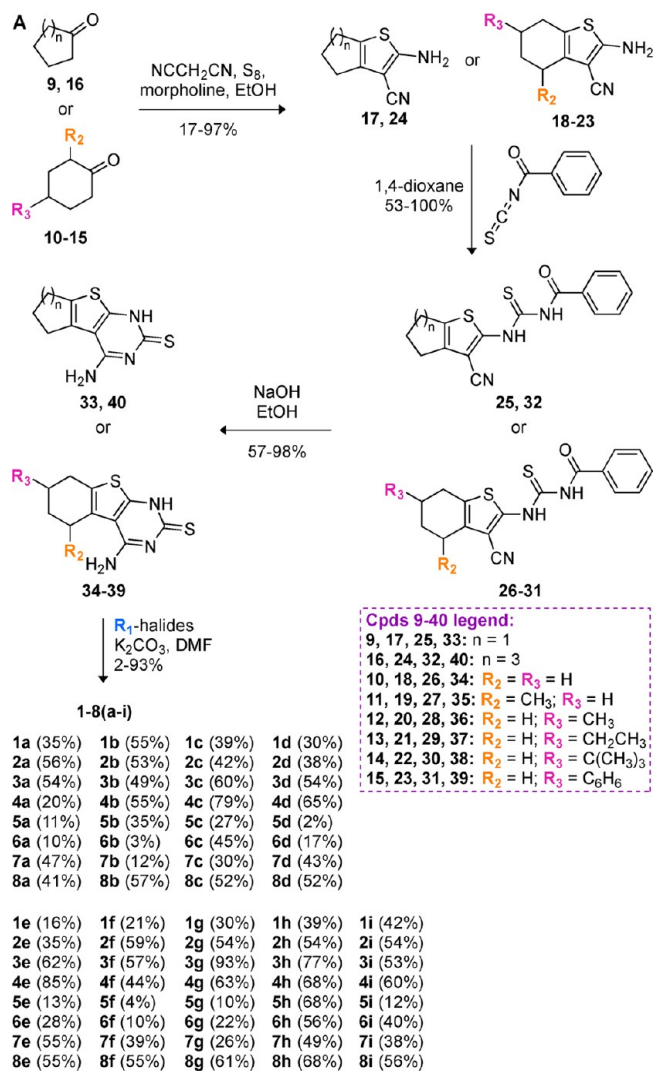
The drastic differences in core orientations, locations of bound water molecules, and consequently the inhibitor–protein interactions, which all arise as a result of seemingly minor chemical differences of the core structures, illustrate potential serious pitfalls of modeling and computational docking based on a crystal structure with a similar pharmacophore. We used the interactions observed in the crystal structure of Eis in a complex with **2i** to design analogues with the thieno[2,3-*d*]pyrimidine-containing core.

**Design and Chemical Synthesis of Eis Inhibitors.** By using the guidelines derived from the crystal structure of the Eis–**2i** complex and its comparison with the structure of Eis–**39b** interactions, as described in the previous section, we made substitutions on the A–B–C core of **2i** (Figure 3; family II) as well on the same thieno[2,3-*d*]pyrimidine B–C core but with a five-membered ring A (Figure 3; family I) as well as a seven-membered ring A (Figure 3; family III). To explore optimal filling in the binding pocket for ring A, we modified ring A with various hydrophobic moieties in family II. In this family, the  $R_3$  position in ring A was unsubstituted (H) or substituted with a methyl, an ethyl, a *tert*-butyl, or a phenyl group (Figure 3). To optimize hydrophobic interactions with residues Met65 and Leu63, we generated molecules in which the  $R_2$  position in ring A was either unsubstituted (H) or substituted with a methyl group. The analogues were divided into eight series (1–8) based on the ring A structure, with family I defining series 1, family II defining series 2–7 with different  $R_2$  and  $R_3$  substituents on ring A, and family III defining series 8. Furthermore, within all eight major series, we also installed side chains  $R_1$  on the sulfur of ring C, in which tertiary amino groups were connected to the sulfur of ring C by an aliphatic linker (with or without an amide), consistent with the restrictions of the narrow binding cleft. These tertiary amines mimic the amino groups of aminoglycoside substrates in the active site, located in the negatively charged environment of the Eis active site (Asp26, Glu401, and the C-terminal carboxyl; Figure 2). We used our previous experience in diversifying substituents at this binding site to install a pyrrolidine or a piperidine, which were observed to improve inhibitor potency in other inhibitors, whereas substituents like carbonyl, hydroxyl, ether, morpholine, or cyano group were not well tolerated.<sup>20</sup> Here, we varied the size of the terminal group on  $R_1$  (for example, a pyrrolidine vs a piperidine ring), the position of the nitrogen, for a constant chain length, the linker length, the presence of an amide bond (imposing constraints in the  $R_1$  side chain and introducing hydrogen bonding potential). A total of nine  $R_1$  variants were generated

as indicated by the letters a–i after the series number. The entire library contained 72 molecules (Figure 3).

To access the thieno[2,3-*d*]pyrimidine core, we initially prepared a series of 2-aminothiophenes (17–24) as building blocks via the classic Gewald aminothiophene synthesis starting from the commercially available malononitrile, sulfur, and various cyclic ketones (9–16) (Scheme 1A). The building

**Scheme 1. Synthetic Scheme for the Preparation of (A) Compounds 1–8(a–i) and (B) Intermediates 41–44**



were not commercially available and were prepared by reacting commercially available primary amines with bromoacetyl chloride (Scheme 1B). The alkyl halides 41–44 were used in alkylation reactions with intermediates 33–40 to afford final products with side chains f, g, h, and i ( $R_1$  groups in Figure 3).

**SAR Deduced from Structural and Functional Studies.** We next sought to identify SAR for the 72 rationally designed Eis inhibitor analogues. The inhibitory potency of the analogues was determined by measuring their effect ( $IC_{50}$ ) on the acetylation of the clinically relevant KAN by Eis (Figure 1; step 5; Table 1 and Figures S225–S228). In order to interpret these data, in addition to the crystal structure of the Eis–2i complex, we determined crystal structures of Eis in complexes with 11 other inhibitors (Tables S1–S3) to avoid making potentially incorrect assumptions based on the structure of Eis in a complex with the parent compound.

**Effect of the Size of Ring A.** The inhibitors with the six-membered ring A were nearly always much more potent Eis inhibitors than those with the five- or the seven-membered ring A and the same  $R_1$  side chain, regardless of the identity of  $R_1$ , whereas the molecules with the seven-membered ring A were generally the least potent of the three (Table 1). This observation explains why most substitutions were made on the six-membered ring (Figure 3; family II). For example, the  $IC_{50}$  values for compounds 1g, 2g, and 8g were  $1.9 \pm 0.6 \mu M$ ,  $0.25 \pm 0.02 \mu M$ , and  $3.1 \pm 0.3 \mu M$ , respectively. To interpret this effect, we determined crystal structures of Eis–1g and Eis–2g complexes (Figure 4). The six-membered ring A of 2g appears to fill the hydrophobic pocket of Eis more efficiently than the five-membered ring of 1g. A  $C_\gamma$  atom of Val40 is  $3.8 \text{ \AA}$  away from the closest C atom of 2g, whereas it is  $4.0 \text{ \AA}$  away in the case of 1g. Analogously, the  $S_\delta$  of Met65 is at  $4.2$  and  $4.3 \text{ \AA}$  from the closest C atoms in 2g and 1g, respectively. These C–C distances are likely optimal for the six-membered ring, and the seven-membered ring of 8g is not accommodated as well.

While this straightforward structural interpretation of the effect of the ring A size on inhibitor potency explains the general trend, there are other consequences to ring A size changes that propagate to the rest of the inhibitor structure and that are not readily interpretable. A subtle ( $0.5 \text{ \AA}$ ) positional shift of the tricyclic cores apparently occurred due to ring A differences, which resulted in different conformations of the  $R_1$  side chain and the side chain of Glu401, as well as differences in water-mediated inhibitor–Eis interactions involving these moieties. The differences in the  $R_1$  conformations resulting from the positional shifts of the cores with different A rings must be responsible in rare cases for the exceptions of the general rank order of potencies for A ring sizes ( $6 > 5 > 7$ ). Such a rare exception was observed for inhibitor 8h with the seven-membered ring, which exhibited the highest potency among the compounds with this  $R_1$  side chain. This potency was similar to that of 2h with the six-membered ring: the  $IC_{50}$  values for 1h, 2h, and 8h were  $2.5 \pm 0.4 \mu M$ ,  $0.46 \pm 0.06 \mu M$ , and  $0.30 \pm 0.06 \mu M$ , respectively.

To investigate this effect in more detail, we determined crystal structures of Eis–1h and Eis–8h complexes (Figure 5). As anticipated, the seven-membered ring A of 8h is bent against the hydrophobic pocket of Eis, and its large size caused a  $0.5 \text{ \AA}$  shift of the thieno[2,3-*d*]pyrimidine core with respect to that of 1h, resulting in a different conformation of  $R_1$ , where it makes additional hydrophobic contacts with the indole ring of Trp36 and positions the tertiary amine of  $R_1$  closer to an  $O_\delta$  of Asp26 (N–O distance of  $3.6 \text{ \AA}$ ) than in 1h (N–O distance of

Table 1. IC<sub>50</sub> and MIC Values<sup>a</sup>

compd	IC <sub>50</sub> (μM)	K204 MIC <sub>KAN</sub> (μg/mL) with 100 μM compd <sup>b</sup>	H37Rv mc <sup>2</sup> 6230 (6206) MIC (μg/mL)	H37Rv mc <sup>2</sup> 6230 (6206) MIC (μM)	compd	IC <sub>50</sub> (μM)	K204 MIC <sub>KAN</sub> (μg/mL) with 100 μM compd <sup>b</sup>	H37Rv mc <sup>2</sup> 6230 (6206) MIC (μg/mL)	H37Rv mc <sup>2</sup> 6230 (6206) MIC (μM)
KAN	N/A	>10, >10 <sup>d</sup>	<1	<1.72	5e	7.0 ± 0.7	10, 10	>128	>340
1a	2.2 ± 0.3	10, 10	8	25	6e	4.6 ± 0.6	toxic	4 (8)	9.9 (20)
2a	0.99 ± 0.06	5, 5	4	12	7e	0.46 ± 0.17	toxic	8	19
3a	6.7 ± 0.7	10, 10	2–4	5.7–12	8e	2.5 ± 0.1	5, toxic	32	88
4a	2.4 ± 0.2	5, 2.5, toxic	4	12	1f	11 ± 1	10, 10	>128	>363
5a	>200	NT	>128	>353	2f	1.5 ± 0.1	5, 5	>128	>350
6a	23 ± 5	toxic	4	10	3f	52 ± 7	>10, >10	>128	>337
7a	4.0 ± 1.1	toxic	4	9.7	4f	3.6 ± 0.4	10, 10	128	337
8a	6.6 ± 0.6	10, >10	4	11	5f	1.1 ± 0.1	NT	64	162
1b	1.9 ± 0.2	5, 5	64	191	6f	~200	NT	>128	>303
2b	1.1 ± 0.1	5, 5	32	92	7f	3.0 ± 0.6	toxic	16	36
3b	14 ± 1	10, 10	32	88	8f	8.7 ± 1.2	10, 10	>100	>263
4b	2.0 ± 0.3	5, 10	8	22	1g <sup>c</sup>	1.9 ± 0.6	NT	>128	>337
5b	5.4 ± 0.5	toxic	4 (8)	11 (21)	2g <sup>c</sup>	0.25 ± 0.02	2.5, 2.5	>128	>325
6b	16 ± 2	toxic	4 (4–8)	9.9 (9.9–20)	3g	~2.4	NT	128	314
7b	16 ± 2	10, 10	16	38	4g	0.20 ± 0.03	5, 2.5	64	157
8b	7.6 ± 1.1	toxic	32	88	5g	1.1 ± 0.2	toxic	16	38
1c <sup>c</sup>	0.75 ± 0.06	2.5, 2.5	32–64	92–183	6g	>200	NT	>128	>284
2c	0.17 ± 0.04	2.5, 2.5	64	176	7g	0.48 ± 0.06	toxic	32	68
3c	3.8 ± 0.5	5, 5, 2.5	16	42	8g	3.1 ± 0.3	5, 5	8	20
4c <sup>c</sup>	0.61 ± 0.08	toxic	16	42	1h <sup>c</sup>	2.5 ± 0.4	5, 5	>128	>327
5c	0.91 ± 0.13	toxic	16	41	2h	0.46 ± 0.06	2.5, 2.5	>128	>315
6c	6.6 ± 1.2	toxic	32	76	3h	6.8 ± 0.6	10, 10	>128	>305
7c <sup>c</sup>	0.23 ± 0.08	toxic	4 (8)	9.1 (18)	4h	3.7 ± 0.6	2.5, 2.5	64	152
8c <sup>c</sup>	1.2 ± 0.1	toxic	16	42	5h <sup>c</sup>	0.68 ± 0.09	toxic	32	74
1d	1.8 ± 0.1	5, 5	16	48	6h	10 ± 4	toxic	16	35
2d	0.45 ± 0.03	5, 5	16	46	7h	0.93 ± 0.29	toxic	8	17
3d	3.6 ± 0.2	2.5, 5	16	44	8h <sup>c</sup>	0.30 ± 0.06	NT	>128	>305
4d	0.81 ± 0.13	toxic	8	22	1i	17 ± 1	5, 5	>128	>325
5d	>200	NT	>128	>340	2i <sup>c</sup>	1.6 ± 0.2	2.5, 2.5	>128	>314
6d	6.3 ± 1.5	toxic	4 (8–16)	9.9 (20–40)	3i	56 ± 6	10, 10	>128	>303
7d	0.53 ± 0.04	NT	16	38	4i	0.47 ± 0.08	1.25, 2.5, 2.5	>100	>237
8d	2.3 ± 0.2	5, 10	16	44	5i	19 ± 3	5, 5	128	294
1e	0.80 ± 0.10	10, 5	128	382	6i	>200	toxic	32	69
2e <sup>c</sup>	0.15 ± 0.02	2.5, 2.5	64	183	7i	16 ± 3	5, toxic, toxic	32	66
3e	2.0 ± 0.1	5, 2.5, 5, 5	64	176	8i	8.5 ± 1.3	5, 5	>128	>303
4e <sup>c</sup>	0.36 ± 0.05	toxic	8	21					

<sup>a</sup>N/A = not applicable; NT = not tested. <sup>b</sup>Multiple MIC values are the results of independent experiments. <sup>c</sup>X-ray structures of Eis in complex with these inhibitors are presented in this study. <sup>d</sup>Note that the MIC of KAN in the parent H37Rv from which the K204 strain is derived is 1.25 μg/mL.

4.2 Å). Shifts in positions of bound waters in the vicinity of this interface were also observed. The significant conformational changes that propagate through the inhibitor and the surrounding solvent, ultimately accounting for the observed effects on inhibitor potency, would not have been possible to model based on the single crystal structure of Eis in a complex with the parent compound or based on molecular docking.

**Effect of Substituents R<sub>2</sub> and R<sub>3</sub> in Family II.** Next, we planned to verify the effect of various substitutions on ring A of the core, by considering the effect of R<sub>2</sub> and R<sub>3</sub> substituents (series 2–7; Figure 3 while keeping the R<sub>1</sub> side chain (a–i) constant. We found that for each R<sub>1</sub>, regardless of its identity, the compounds with no substituents at R<sub>2</sub> and R<sub>3</sub> (series 2) were nearly always the most potent. Even the small methyl group at R<sub>2</sub> (series 3) was not tolerated, generally resulting in at least a 10-fold higher IC<sub>50</sub> value than that of its unsubstituted counterpart from series 2. Indeed, the methyl group at R<sub>2</sub>, depending on the stereoconfiguration, would sterically clash with the S<sub>γ</sub> of Met65 or with the C<sub>β</sub> atom of

Phe84, because the distances from the C atom of the core and the respective S<sub>γ</sub> and C<sub>β</sub> are 4.2 and 4.1 Å along the potential C–C bond between the core and the R<sub>2</sub> methyl group (Figure 4B). Nonpolar substituents, such as a methyl, an ethyl, and a phenyl group at R<sub>3</sub>, were well tolerated while a *tert*-butyl substituent was the least tolerated, regardless of R<sub>1</sub> (Table 1). The relatively small methyl and ethyl substituents at R<sub>3</sub> were predicted to be less hindered than at R<sub>2</sub>, because in either stereoconfiguration they would not clash with the protein (Figure 4B). Furthermore, the flexible side chain of Arg37 could change its conformation to enlarge the binding pocket. On the other hand, a *tert*-butyl group (series 6) or a phenyl ring (series 7) would not be readily accommodated. Indeed, series 6 nearly always contained the least potent compounds. Unexpectedly, some of compounds in series 7 were highly potent Eis inhibitors. To learn about the structural consequences of a methyl substitution at R<sub>3</sub>, we determined crystal structures of Eis in complexes with highly potent inhibitors 2e (IC<sub>50</sub> = 0.15 ± 0.02 μM; PDB ID 6VUR) and 4e

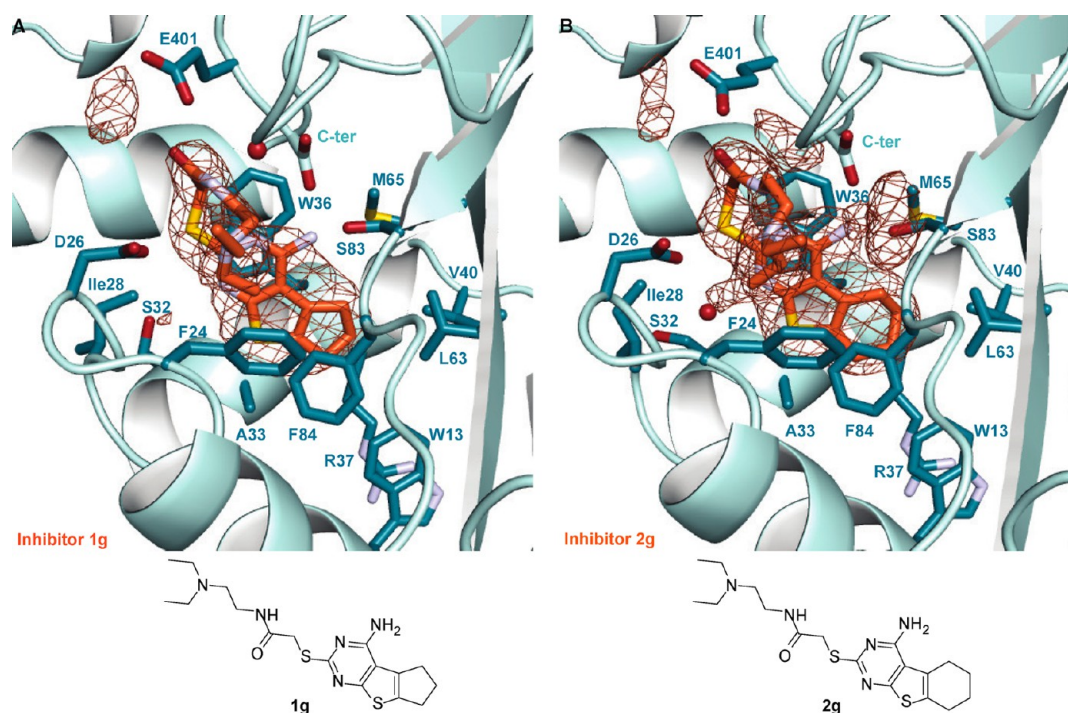


**Figure 4.** Zoomed-in views of the Eis–inhibitor interfaces from crystal structures of Eis–1g and Eis–2g complexes, and the inhibitor structures: (A) Eis–1g interface and (B) Eis–2g interface.

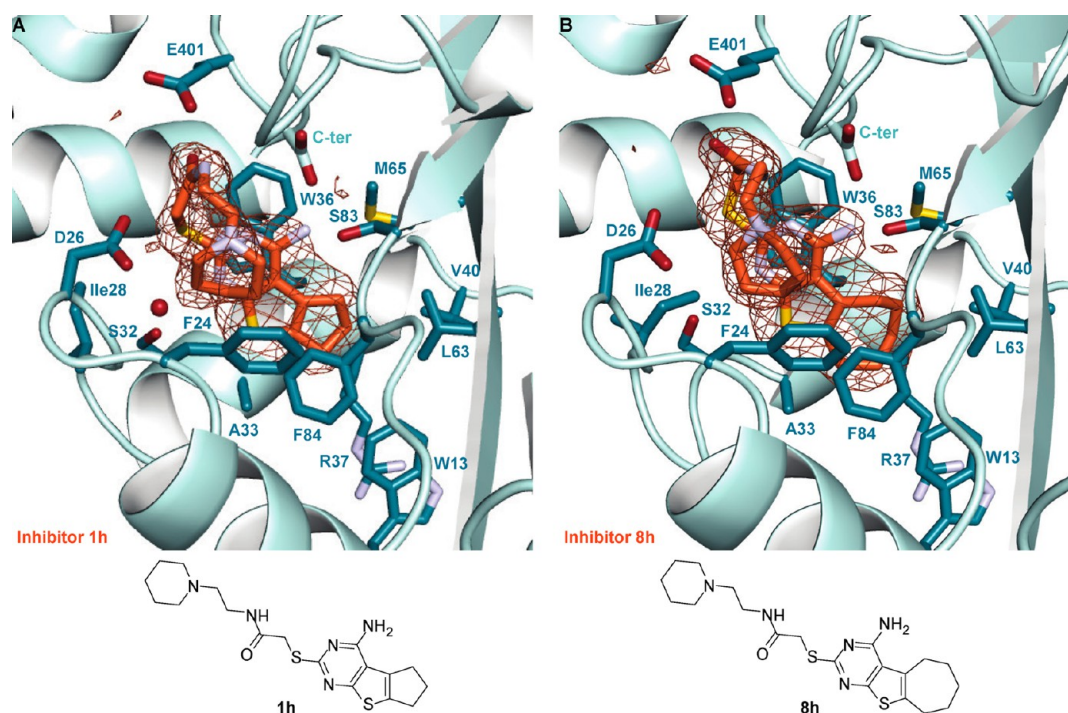


**Figure 5.** Zoomed-in views of the Eis–inhibitor interfaces from crystal structures of Eis–1h and Eis–8h complexes and the inhibitor structures. (A) Eis–1h interface and (B) Eis–2h interface.

( $IC_{50} = 0.36 \pm 0.05 \mu\text{M}$ ; PDB ID 6VUW), which differ from each other only by the presence of a methyl group at  $R_3$  in **4e** (Figure 6). As anticipated, the methyl group was accommodated largely owing to a change of the conformation of the side chain of Arg37 and a minor shift by 0.4 Å of the inhibitor. The methyl group interacts favorably with Arg37 and Trp13, with the closest C–C distances of 3.8 and 3.6 Å, respectively. To investigate how a bulky phenyl group was accommodated

at  $R_3$ , we determined a crystal structure of Eis in a complex with the most potent inhibitor in series 7, **7c** ( $IC_{50} = 0.23 \pm 0.08 \mu\text{M}$ ; PDB ID 6VUY; Figure 7A). As expected, large conformational changes had to occur to fit the phenyl group into the binding pocket. The indole ring of Trp13 rotated by  $90^\circ$  around the  $C_\beta$ – $C_\gamma$  bond and stacked orthogonally against the  $R_3$  phenyl group of **7c**. In turn, the side chain of Arg37 changed conformation to stack orthogonally with the indole of

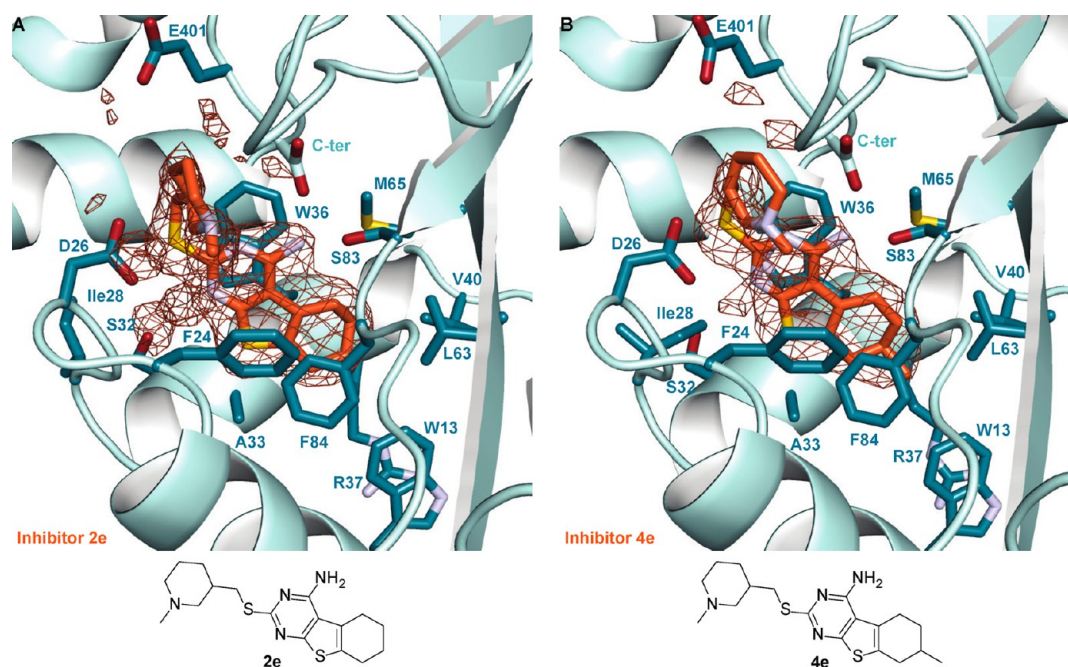


**Figure 6.** Zoomed-in views of the Eis–inhibitor interfaces from crystal structures of Eis–2e and Eis–4e complexes and the inhibitor structures: (A) Eis–2e interface and (B) Eis–4e interface.

Trp13 against its edge. Notably, computational molecular docking, which relies heavily on rigid-body assumptions, would not predict that 7c is a potent inhibitor of Eis.

**Effects of  $R_1$  Substituents for Each of the Three Inhibitor Families.** The effect of different  $R_1$  substituents is complex, because the  $R_1$  side chain is extended into a large hydrophilic cleft lined with polar and charged residues. SAR have emerged, as follows.

**a. Effect of the Ring Size at the Terminus of  $R_1$ .** First, we investigated an effect of a terminal pyrrolidine ( $R_1 = \mathbf{a}$ ) vs a piperidine ring ( $R_1 = \mathbf{b}$ ) for the same 2-carbon linker. These substituents generally did not lead to significant improvement in potency from that of the parent compound 2i. In families I and III and in series 2 and 4 of family II, the  $R_1$  ring size had no effect. In the rest of the series of family II the effect was generally 2-fold or greater, favoring either the five- or the six-membered ring. In all of these last cases, the inhibitors had relatively low potencies (in the  $IC_{50}$  range from  $4.0 \pm 1.1 \mu\text{M}$  to  $>200 \mu\text{M}$ ).

**b. Effect of the Length of the Linker in  $R_1$ .** To test the impact of the length of the  $R_1$  linker, we compared compounds with a 2-carbon linker to those with a 3-carbon  $R_1$  linker, both containing a terminal piperidine ring (series **b** vs **c**). The longer, 3-carbon linker ( $R_1 = \mathbf{c}$ ), was strongly favored over the 2-carbon linker ( $R_1 = \mathbf{b}$ ) in all three families (Table 1). In order to visualize the structural basis for this significant improvement, in addition to Eis–7c, we determined crystal structures of Eis in complexes with three additional potent inhibitors: 1c ( $IC_{50} = 0.75 \pm 0.06 \mu\text{M}$ ; PDB ID 6VUZ), 4c ( $IC_{50} = 0.61 \pm 0.08 \mu\text{M}$ ; PDB ID 6VUU), and 8c ( $IC_{50} = 1.2 \pm 0.1 \mu\text{M}$ ; PDB ID 6VV2) (Figure 7). These structures revealed that this longer  $R_1$  linker places the positively charged amino group of the piperidine so that it is equidistant from the carboxyl groups of Asp26, Glu401, and the C-terminal carboxyl group, all three at appropriate distances for strong salt bridge formation. The piperidine ring was found in different

conformations, all related by rotations along the C–N bond connecting the ring to the  $R_1$  linker.

**c. Effect of the Position of the Tertiary Amino Group in  $R_1$ .** Since all  $R_1$  side chains contain a tertiary amino group in them, we examined the impact of the position of the tertiary amino group in the pyrrolidine ring on the potency of the compounds ( $R_1 = \mathbf{a}$  vs **d**). We observed that the ring nitrogen that is not directly attached to the 2-carbon linker ( $R_1 = \mathbf{d}$ ) is preferred (Table 1). Having noted this, we then asked if we could further improve potency by keeping four bonds between the ring nitrogen and the core but enlarging the  $R_1$  ring to the piperidine ( $R_1 = \mathbf{d}$  vs **e**). In all but two series, 7 and 8, the inhibitors with the piperidine ring (**e**) were more potent than those with the pyrrolidine ring (**d**), and for series 7 and 8 the potency was not affected. The crystal structures of Eis–2e and Eis–4e complexes (Figure 6) showed that in series **e**, the tertiary amino group is placed directly between the carboxyl groups of Asp26 and the C-terminus for salt bridge formation, whereas the aliphatic side of the appropriately sized piperidine ring interacts with the aliphatic portion of the side chain of Glu401, explaining the observed trend of potencies.

**d. Substituents with an Amide in  $R_1$ .** We explored a potential benefit from further lengthening of an  $R_1$  linker and an introduction of an amide into it, to add polar character. In addition, we assessed the variability of the terminal  $R_1$  groups, which included a dimethyl amine (**f**), a diethyl amine (**g**), a piperidine (**h**), and a morpholine (**i**) groups. The compounds with a diethyl amino group (**g**) and a piperidine ring (**h**) were more potent than those with the other two choices of the  $R_1$  termini (Table 1). To examine the interactions of side chains **g** and **h** with Eis, in addition to the structures of Eis in complex with the potent inhibitors 2g (Figure 4B) and 8h (Figure 5B) described above, we determined the crystal structure of Eis in complex with inhibitor 5h ( $IC_{50} = 0.68 \pm 0.09 \mu\text{M}$ ; PDB ID 6VUX; Figure 8), the most potent inhibitor in series 5. Apparently, the side chain  $R_1 = \mathbf{h}$  overcame the unfavorable effect of the ethyl group at  $R_3$  observed with other choices of

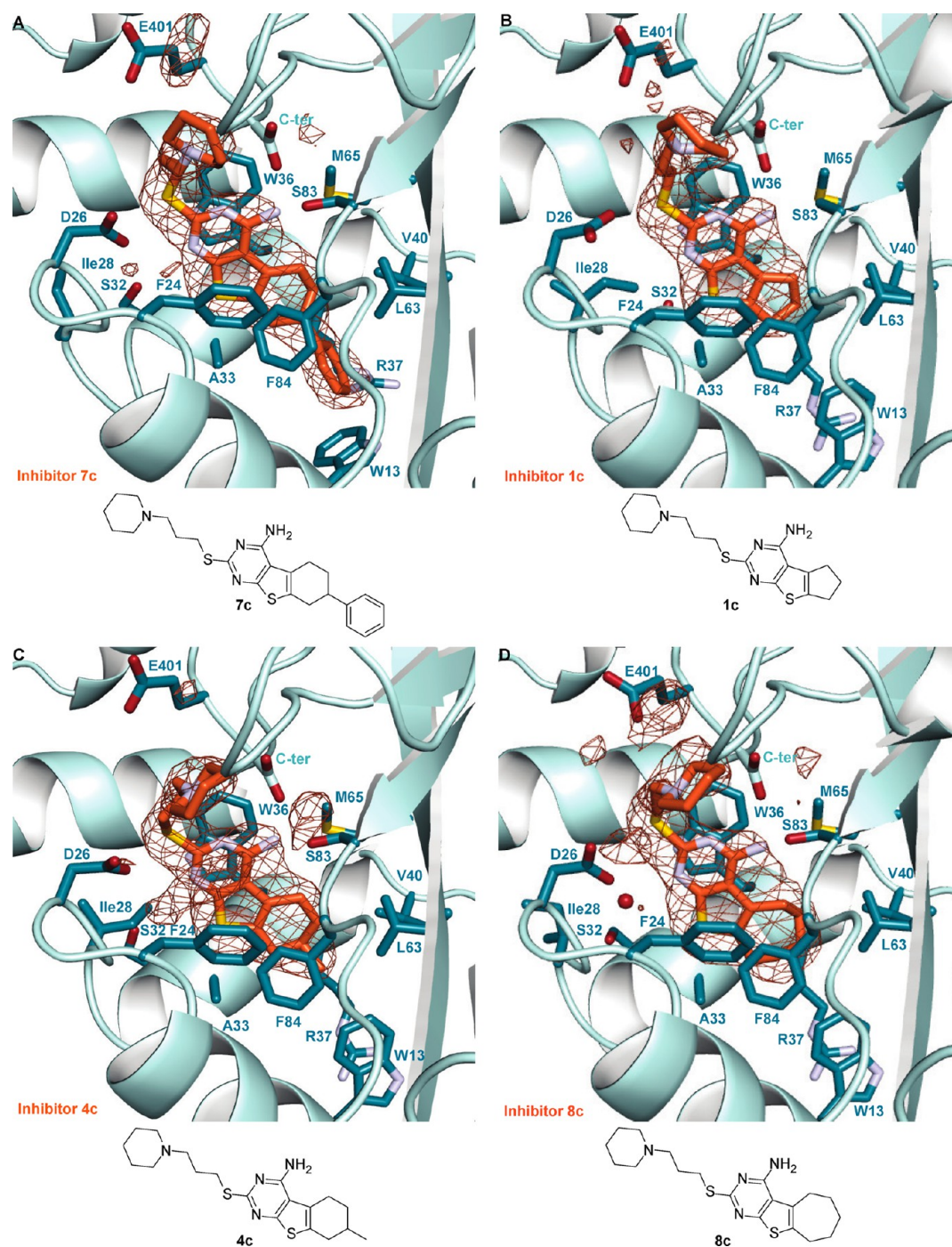


**Figure 7.** Zoomed-in views of the Eis–inhibitor interfaces from crystal structures of Eis–7c, Eis–1c, Eis–4c, and Eis–8c complexes and the inhibitor structures: (A) Eis–7c interface, (B) Eis–1c interface, (C) Eis–4c interface, and (D) Eis–8c interface.

$R_1$  in this series. Analogously, the side chain  $R_1 = \mathbf{h}$  was the most favored in family 8. In all these three structures, the  $R_1$  side chain is in the same U-turn conformation, where the thioether moiety is coplanar with the tricyclic core and the amide is solvent exposed. The tertiary amino group formed a salt bridge with Asp26. The diethyl group of **2g** and the piperidine rings of **5h** and **8h** abutted the phenyl ring of Phe24, explaining why the morpholine ring in series **i** containing a polar oxygen was less preferred. The rigidity of the amide-containing linker and the restraint imposed by Phe24 likely accounted for the high potency of these molecules. Other structural factors seemed to modulate the potency. For

example, the ethyl group at  $R_3$  of **5h** wedged against Trp13 and Arg37, pushing the latter off and compromising its stacking against Trp13, likely caused a 2-fold weaker potency of this analogue than those of the equipotent **2g** and **8h**, in which ring A was unsubstituted.

**Buried Surface Area of Eis–Inhibitor Complexes.** Binding of macromolecules to each other and to druglike molecules commonly depends on geometrical and physical complementarity of the two interacting interfaces. Upon such binding, water is excluded from the interface between the nonpolar surfaces, providing a favorable entropic contribution in addition to the favorable van der Waals energy gain by the

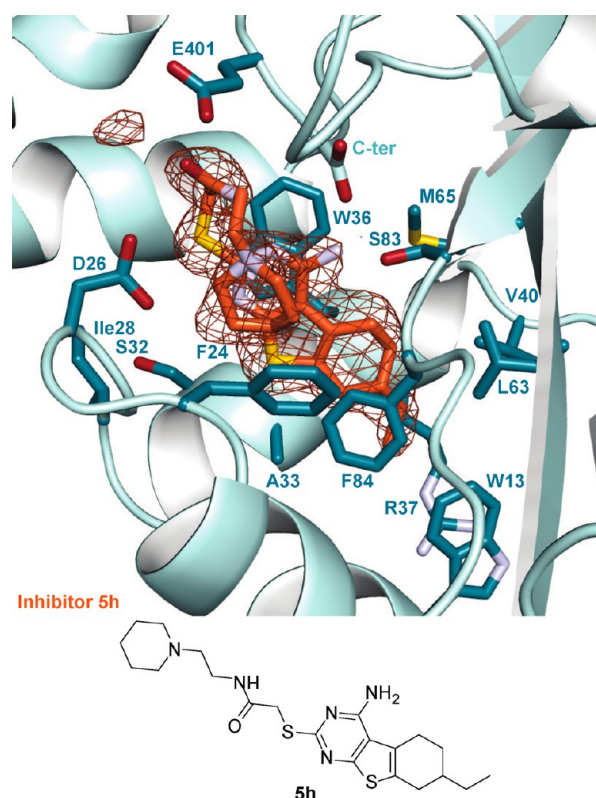


**Figure 8.** Zoomed-in view of the Eis–inhibitor interface from crystal structure of Eis–5h complex and the structure of 5h.

contact of the two properly spaced surfaces. Formation of the interface between the two polar or charged surfaces, in addition to the geometrical complementarity similarly needed to ensure favorable van der Waals interactions, requires that the energy stored in hydrogen bonds and salt bridges involved in hydration and solvation of such surfaces is not lost upon binding. Therefore, one can observe that in the interfaces between polar surfaces buried from bulk solvent, hydrogen bonds, and salt bridges are formed across the interface (when solvent is also excluded with a favorable gain of entropy) or with water molecules or ions trapped in the interface, without losing these energetically costly interactions. With the benefit of obtaining a set of crystal structures of Eis in complexes with 12 inhibitors, we calculated<sup>23</sup> the total solvent accessible surface area buried in the interface between the protein and the inhibitors ( $ASA_{b,t}$ ) and examined whether there is any trend in the inhibitor potency with respect to  $ASA_{b,t}$ . We also considered separately the buried nonpolar ( $ASA_{b,np}$ ) and polar ( $ASA_{b,p}$ ) surface areas (Figure S229).  $ASA_{b,np}$  comprised approximately two-thirds of  $ASA_{b,t}$  and, as expected based on the complementarity principles discussed above, was the dominant contribution to the trend in  $ASA_{b,t}$  with respect to  $IC_{50}$ . The larger  $ASA_{b,t}$  and  $ASA_{b,np}$  were associated with higher potency (smaller  $IC_{50}$  values), underscoring the importance of hydrophobic interactions, although the correlation was relatively weak:  $R = 0.040$  and  $-0.259$ , respectively. To our surprise,  $ASA_{b,p}$  had a stronger correlation with the opposite trend ( $R = 0.691$ ), where the larger  $ASA_{b,p}$  were associated with lower potency. We interpreted this to mean that in burying polar surfaces, the resulting hydrogen bonds and salt bridges in the interface were not as favorable as those with bulk solvent in the unbound state. Additionally, the loss of the

conformational freedom of the polar and charged side chains upon inhibitor binding may be another contributor. These calculations are consistent with the notion that the interactions between complementary nonpolar surfaces are drivers of inhibitor potency and they advocate for frugal and rational incorporation of polar and charge groups.

**Competitive Inhibition Mode.** All 12 crystal structures of Eis–inhibitor complexes presented here show that the inhibitors are bound at the Eis active site in the pocket that overlaps with the aminoglycoside substrate binding pocket (Figure S224), strongly suggesting that these molecules inhibit the acetyl transfer by competing with the aminoglycosides for binding Eis. We tested this directly by monitoring kinetics of acetylation of KAN by Eis in the steady-state, as a function of KAN in the absence of the inhibitor and at several concentrations of each of three potent inhibitors, 4c, 7c, and 4g (Figure 9). These data show that, within experimental uncertainty, these inhibitors display a competitive (with respect to KAN) inhibition mode, in agreement with the crystal structures. The global fit of the competitive mode of inhibition to these data yielded the  $K_i$  values for these three inhibitors (Table 2), all in the 0.15–0.34  $\mu\text{M}$  range.

**Effect of Inhibitors on the  $MIC_{KAN}$  against *Mtb* in Vitro.** In addition to the parent inhibitor 2i, we measured the effect of other Eis inhibitors at 100  $\mu\text{M}$  on KAN resistance caused by Eis overexpression (Table 1). Inhibitors that had relatively low potencies ( $IC_{50} > 10 \mu\text{M}$ ) generally had no effect on the  $MIC_{KAN}$  of the KAN-resistant *Mtb* strain K204, whereas compounds that were highly potent generally lowered the  $MIC_{KAN}$  as much as 4-fold, to 2.5  $\mu\text{g/mL}$ . Intriguingly, while many of the compounds did not affect the growth of *Mtb* K204 in the absence of KAN, several compounds from families II and III were toxic (at  $MIC < 100 \mu\text{M}$ ) to this strain even in the absence of KAN, which means that the compounds act via an additional mechanism besides Eis inhibition. This unknown mechanism merits investigation in the future. As a control, we also determined MIC values of all the inhibitors in the absence of KAN against another *Mtb* strain that contained the wild-type *eis* promoter, H37Rv mc<sup>2</sup> 6230 (Table 1). In agreement with the inhibitory effect on growth of *Mtb* K204, these compounds displayed  $MIC < 100 \mu\text{M}$ , some inhibitors as low as 9  $\mu\text{M}$ . Five of the molecules were also tested against the culture of another H37Rv variant, mc<sup>2</sup> 6206. These MIC values were comparable to those for *Mtb* H37Rv mc<sup>2</sup> 6230 (Table 1).

**Mammalian Cytotoxicity.** The cytotoxic effect of three Eis inhibitors and KAN was evaluated against three mammalian cell lines: human adenocarcinoma (A549), human embryonic kidney (HEK-293), and mouse macrophage (J774A.1) (Figure 10 and Figure S230). Inhibitors 2e and 2i were chosen as at 100  $\mu\text{M}$  they restore the activity of KAN in *Mtb* K204 (Table 1). Compound 7c was chosen as it is toxic to *Mtb* strains with MIC values of 4 and 8  $\mu\text{M}$  for strains H37Rv mc<sup>2</sup> 6230 and mc<sup>2</sup> 6206, respectively. We observed that 7c displayed toxicity against all three cell lines at 25  $\mu\text{M}$ . Against A549 cells, 7c displayed no toxicity at 6.3  $\mu\text{M}$  and approximately 20% cell survival at 12.5  $\mu\text{M}$ . Similarly, against the J774A.1 cell line, no toxicity was observed up to 3.1  $\mu\text{M}$ , with 30% cell survival at 6.3  $\mu\text{M}$ . These values are very similar to the concentrations that are toxic to both strains of *Mtb* tested. In contrast, inhibitors 2e and 2i displayed no toxic effect at the highest concentration tested, 50  $\mu\text{M}$ , which is highly promising.

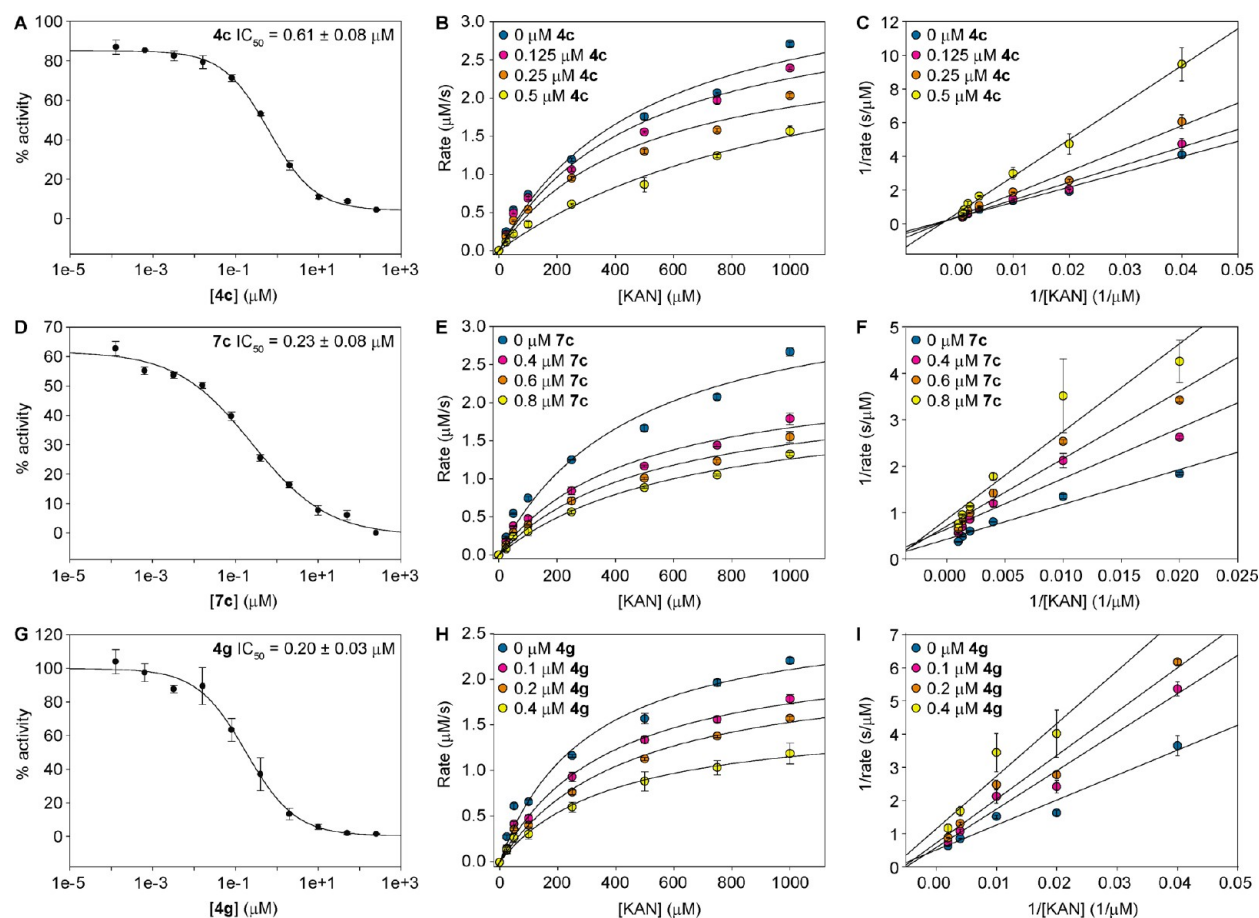


**Figure 9.** Analysis of inhibition kinetics for inhibitors **4c**, **7c**, and **4g**. Dose–response curves are shown in panels A, D, and G; Michaelis–Menten analysis is in panels B, E, and H; and the Lineweaver–Burk representation of this analysis is in panels C, F, and I. These data indicate that the molecules are competitive with KAN. These data are used in obtaining  $K_i$  by global nonlinear regression (Table 2).

**Table 2.** Kinetic Parameters of Eis and  $K_i$  Values for Inhibitors **4c**, **4g**, and **7c**

cmpd	[inhibitor] ( $\mu\text{M}$ )	$K_{m,\text{KAN}}$ ( $\mu\text{M}$ )	$k_{\text{cat}}$ ( $\text{s}^{-1}$ )	$k_{\text{cat}}/K_{m,\text{KAN}}$ ( $\text{s}^{-1} \mu\text{M}^{-1}$ )	$K_i$ ( $\mu\text{M}$ )
<b>4c</b>	0	$460 \pm 150$	$14 \pm 2$	$0.031 \pm 0.01$	$0.34 \pm 0.02$
	0.4	$460 \pm 120$	$9.8 \pm 1.2$	$0.021 \pm 0.006$	
	0.6	$530 \pm 120$	$8.9 \pm 1.0$	$0.017 \pm 0.005$	
	0.8	$650 \pm 150$	$8.3 \pm 1.0$	$0.013 \pm 0.003$	
<b>4g</b>	0	$310 \pm 74$	$11 \pm 1$	$0.036 \pm 0.009$	$0.15 \pm 0.01$
	0.1	$370 \pm 59$	$9.6 \pm 0.6$	$0.027 \pm 0.004$	
	0.2	$440 \pm 82$	$8.8 \pm 0.7$	$0.020 \pm 0.004$	
	0.4	$390 \pm 64$	$6.4 \pm 0.4$	$0.016 \pm 0.003$	
<b>7c</b>	0	$510 \pm 160$	$15 \pm 2$	$0.029 \pm 0.01$	$0.31 \pm 0.03$
	0.125	$500 \pm 140$	$14 \pm 2$	$0.027 \pm 0.008$	
	0.25	$490 \pm 140$	$11 \pm 1$	$0.022 \pm 0.007$	
	0.5	$1200 \pm 400$	$13 \pm 3$	$0.011 \pm 0.004$	

**Microsomal Stability.** In any drug discovery process, preclinical drug metabolism assessment plays a vital role in drug optimization. We tested the metabolic stability in human and mouse microsomes of several compounds in family II that were selected to represent the structural diversity of the family and predicted as stable by using StarDrop software (Optibrium) (Table 3). As expected, stabilities in human microsomes were grouped according to the nature of the  $R_1$  side chain, whereas in mouse microsomes most compounds were quite labile. Two compounds (**6i** and **7i**) were completely metabolized by both human and mouse microsomes, while most of the other tested compounds were modestly

metabolized by human microsomes. For these and several other molecules, the metabolic liability can be predicted. The instability of **7i** may be due to the presence of an unsubstituted phenyl ring with oxidation at the para position of the phenyl ring or on the morpholine ring as well as hydrolysis of the amide bond. Similarly, **6i** could be metabolized by oxidation at three major sites, namely, the *tert*-butyl group, the amide linker, and the sulfur linkage. Several compounds showed moderate stability (25–40% metabolized) with human microsomes (**7a**, **4c**, **4d**, **7e**). Metabolism of **4d**, **6d**, and **7e** is likely to be demethylation. Several compounds had improved stability with <25% metabolized in human microsomes (**6a**,

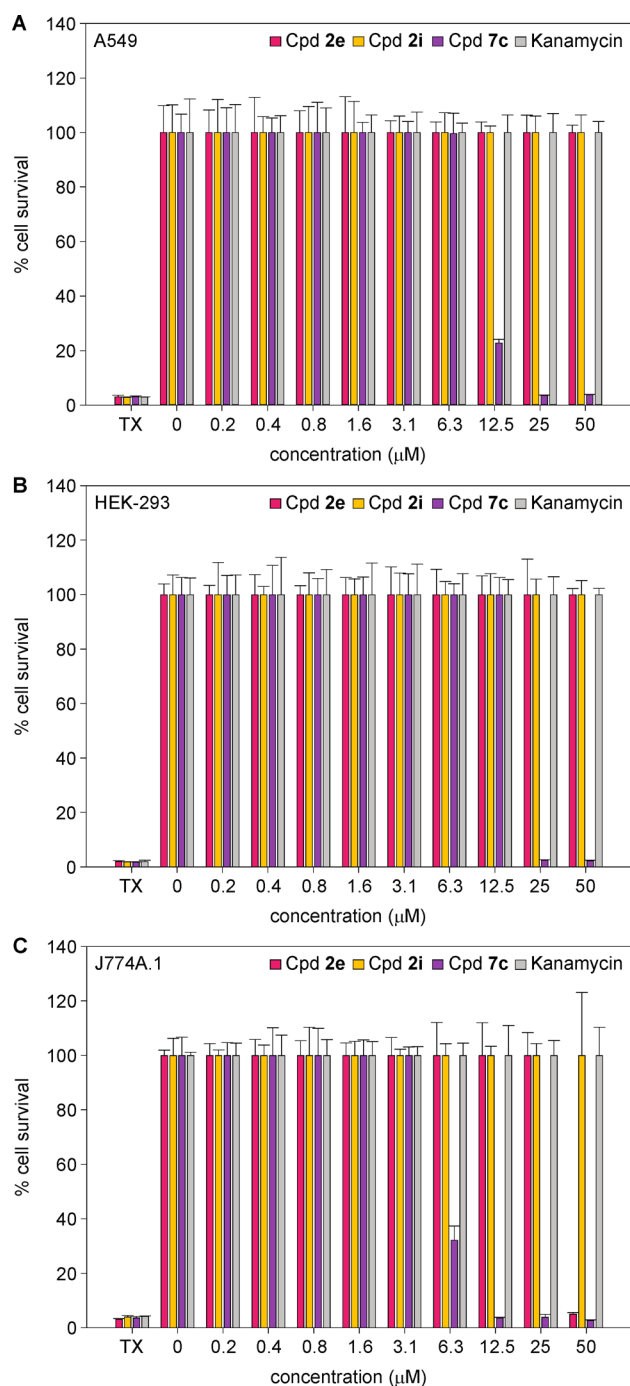


**Figure 10.** Evaluation of cytotoxicity for compounds **2e** (red), **2i** (yellow), **7c** (purple), and KAN (gray) against three cell lines: (A) A549, (B) HEK-293, and (C) J774A.1. Controls include treatment with Triton-X (TX, 1% v/v, positive control) and 0.5% DMSO (negative control). It is important to note that testing xenobiotics at sub-IC<sub>50</sub> concentrations can result in increase in cell growth, resulting in >100% cell survival in the treatment groups. In instances where >100% cell survival was observed, we displayed the data as 100% cell survival. Note: The raw data are presented in Figure S230.

**5c**, **7c**, **6d**). The molecules that were most labile in the human microsomes were also highly labile in the mouse microsomes, but the converse was not true. For example, **6d** and **5c** were stable with human microsomes (20% and 7%, respectively), but not with mouse microsomes (62% and 52%, respectively).

**Table 3.** Metabolic Stability of Eis Inhibitors

inhibitor	human	mouse
<b>6a</b>	23 ± 21 <sup>a</sup>	53 ± 5
<b>7a</b>	36 ± 24	38 ± 16
<b>4c</b>	31 ± 4	99 ± 0
<b>5c</b>	7 ± 5	52 ± 21
<b>7c</b>	22 ± 2	47 ± 25
<b>4d</b>	38 ± 6	99 ± 0
<b>6d</b>	20 ± 2	62 ± 16
<b>7e</b>	38 ± 4	75 ± 3
<b>7h</b>	47 ± 5	58 ± 4
<b>6i</b>	100 ± 0	100 ± 0
<b>7i</b>	94 ± 7	100 ± 0

<sup>a</sup>The values in the table are % metabolized compound after a 30 min incubation with microsomes. The data are the mean ± standard deviation for a minimum of three samples (except **4d**, which was tested in duplicates).

## CONCLUSION

A new class of Eis inhibitors having thieno[2,3-*d*]pyrimidine core was discovered, with various analogues synthesized and rationally optimized guided by structural studies, followed by their extensive characterization using chemical, biochemical, structural, and biological studies. Several analogues with potent inhibitory activity against purified Eis were able to restore the MIC<sub>KAN</sub> in cellular assays, while displaying no toxicity against either *Mtb* or mammalian cells on their own. For compounds that displayed toxicity against *Mtb*, it remains to be investigated whether all these compounds are also toxic to mammalian cells (inhibitor **7c** is toxic to both). *In vitro* metabolism assays show that several side chains were tolerated well metabolically, with R<sub>1</sub> = **c** being especially promising. Pending further toxicity testing, compounds **1c** and **2c**, which are nontoxic to *Mtb* on their own, but potent in Eis inhibition and synergistic with KAN, emerged as promising compounds for further testing.

## EXPERIMENTAL SECTION

Details of all experimental procedures for synthesis and characterization of all compounds and intermediates, HTS, hit validation, selectivity of inhibitors toward Eis, *Mtb* MIC value determination, dose-dependent *Mtb* MIC values determination, crystallization, and crystal structure determination of Eis–inhibitor complexes, solvent accessible surface area calculations, and metabolic stability assays are included in the Supporting Information. The Supporting Information also includes all <sup>1</sup>H and <sup>13</sup>C NMR spectra as well as HPLC traces for the molecules generated (Figures S1–S222).

## ASSOCIATED CONTENT

### Supporting Information

The Supporting Information is available free of charge at <https://pubs.acs.org/doi/10.1021/acscchembio.0c00184>.

Additional details of the chemistry and the biochemical, biological, and biophysical assays (PDF)

### Accession Codes

PDB accession codes: Eis–**1c** (6VUZ), Eis–**1g** (6VV0), Eis–**1h** (6VV1), Eis–**2e** (6VUR), Eis–**2g** (6VUS), Eis–**2i** (6VUT), Eis–**4c** (6VUU), Eis–**4e** (6VUW), Eis–**5h** (6VUX), Eis–**7c** (6VUY), Eis–**8c** (6VV2), Eis–**8h** (6VV3).

## AUTHOR INFORMATION

### Corresponding Authors

**Sylvie Garneau-Tsodikova** – Department of Pharmaceutical Sciences, University of Kentucky, Lexington, Kentucky 40536-0596, United States; [orcid.org/0000-0002-7961-5555](https://orcid.org/0000-0002-7961-5555); Phone: 859-218-1686; Email: [sylviegttsodikova@uky.edu](mailto:sylviegttsodikova@uky.edu)

**Oleg V. Tsodikov** – Department of Pharmaceutical Sciences, University of Kentucky, Lexington, Kentucky 40536-0596, United States; [orcid.org/0000-0001-7094-4216](https://orcid.org/0000-0001-7094-4216); Phone: 859-218-1687; Email: [oleg.tsodikov@uky.edu](mailto:oleg.tsodikov@uky.edu)

### Authors

**Ankita Punetha** – Department of Pharmaceutical Sciences, University of Kentucky, Lexington, Kentucky 40536-0596, United States

**Huy X. Ngo** – Department of Pharmaceutical Sciences, University of Kentucky, Lexington, Kentucky 40536-0596, United States

**Selina Y. L. Holbrook** – Department of Pharmaceutical Sciences, University of Kentucky, Lexington, Kentucky 40536-0596, United States

**Keith D. Green** – Department of Pharmaceutical Sciences, University of Kentucky, Lexington, Kentucky 40536-0596, United States

**Melisa J. Willby** – Division of Tuberculosis Elimination, National Center for HIV/AIDS, Viral Hepatitis, STD, and TB Prevention, Centers for Disease Control and Prevention, Atlanta, Georgia 30333, United States

**Shilah A. Bonnett** – TB Discovery Research, Infectious Disease Research Institute, Seattle, Washington 98102, United States

**Kyle Krieger** – TB Discovery Research, Infectious Disease Research Institute, Seattle, Washington 98102, United States; Center for Global Infectious Disease, Seattle Children's Research Institute, Seattle Children's Hospital, Seattle, Washington 98145, United States

**Emily K. Dennis** – Department of Pharmaceutical Sciences, University of Kentucky, Lexington, Kentucky 40536-0596, United States

**James E. Posey** – Division of Tuberculosis Elimination, National Center for HIV/AIDS, Viral Hepatitis, STD, and TB Prevention, Centers for Disease Control and Prevention, Atlanta, Georgia 30333, United States

**Tanya Parish** – TB Discovery Research, Infectious Disease Research Institute, Seattle, Washington 98102, United States; Center for Global Infectious Disease, Seattle Children's Research Institute, Seattle Children's Hospital, Seattle, Washington 98145, United States

Complete contact information is available at:

<https://pubs.acs.org/10.1021/acscchembio.0c00184>

### Author Contributions

<sup>†</sup>A.P. and H.X.N. contributed equally to this work.

### Notes

The authors declare no competing financial interest.

## ACKNOWLEDGMENTS

This study was funded by a National Institutes of Health (NIH) Grant AI090048 (to S.G.-T.), a grant from the Firland Foundation (to S.G.-T.), a grant from the Center for Chemical Genomics (CCG) at the University of Michigan (to S.G.-T.), as well as by startup funds from the College of Pharmacy at the University of Kentucky (to S.G.-T. and O.V.T.). We thank the

UK PharmNMR Center (in the College of Pharmacy) for NMR support and S. Van Lanen for managing the LCMS system used in this study. We thank S. Vander Roest, M. Larsen, and P. Kirchoff from the CCG at the University of Michigan for their help with HTS. We thank J. J. Johnson and R. M. Holmes for synthesizing and characterizing a few of the molecules presented in this manuscript. We thank C. Hou for assistance with the protein purification and crystallization. We also thank S. Chowdhury and B. Berube for discussion and technical assistance with metabolic stability assays. Use of trade names is for identification only and does not constitute endorsement by the U.S. Department of Health and Human Services, the U.S. Public Health Service, or the CDC. The findings and conclusions in this report are those of the authors and do not necessarily represent the views of the funding agency.

## ABBREVIATIONS

AcCoA, acetyl coenzyme A; ASA, accessible surface area; Eis, enhanced intracellular survival; HPLC, high-performance liquid chromatography; HTS, high-throughput screening; IC<sub>50</sub>, inhibitory concentration at half-maximum inhibition; KAN, kanamycin; MDR, multidrug-resistant; MIC, minimum inhibitory concentration; *Mtb*, *Mycobacterium tuberculosis*; PDB, Protein Data Bank; SAR, structure–activity relationship; TB, tuberculosis; XDR, extensively drug-resistant

## REFERENCES

- (1) Rice, L. B. (2008) Federal funding for the study of antimicrobial resistance in nosocomial pathogens: no ESKAPE. *J. Infect. Dis.* 197, 1079–1081.
- (2) *Global Tuberculosis Report 2019*, World Health Organization, Geneva, Switzerland, 2019, licence CCBY-NC-SA3.01GO.
- (3) Zaunbrecher, M. A., Sikes, R. D., Jr., Metchock, B., Shinnick, T. M., and Posey, J. E. (2009) Overexpression of the chromosomally encoded aminoglycoside acetyltransferase *eis* confers kanamycin resistance in *Mycobacterium tuberculosis*. *Proc. Natl. Acad. Sci. U. S. A.* 106, 20004–20009.
- (4) Campbell, P. J., Morlock, G. P., Sikes, R. D., Dalton, T. L., Metchock, B., Starks, A. M., Hooks, D. P., Cowan, L. S., Plikaytis, B. B., and Posey, J. E. (2011) Molecular detection of mutations associated with first- and second-line drug resistance compared with conventional drug susceptibility testing of *Mycobacterium tuberculosis*. *Antimicrob. Agents Chemother.* 55, 2032–2041.
- (5) Reeves, A. Z., Campbell, P. J., Sultana, R., Malik, S., Murray, M., Plikaytis, B. B., Shinnick, T. M., and Posey, J. E. (2013) Aminoglycoside cross-resistance in *Mycobacterium tuberculosis* due to mutations in the 5' untranslated region of *whiB7*. *Antimicrob. Agents Chemother.* 57, 1857–1865.
- (6) Chen, W., Biswas, T., Porter, V. R., Tsodikov, O. V., and Garneau-Tsodikova, S. (2011) Unusual regioversatility of acetyltransferase Eis, a cause of drug resistance in XDR-TB. *Proc. Natl. Acad. Sci. U. S. A.* 108, 9804–9808.
- (7) Chen, W., Green, K. D., Tsodikov, O. V., and Garneau-Tsodikova, S. (2012) Aminoglycoside multiacetylating activity of the enhanced intracellular survival protein from *Mycobacterium smegmatis* and its inhibition. *Biochemistry* 51, 4959–4967.
- (8) Houghton, J. L., Biswas, T., Chen, W., Tsodikov, O. V., and Garneau-Tsodikova, S. (2013) Chemical and structural insights into the regioversatility of the aminoglycoside acetyltransferase Eis. *ChemBioChem* 14, 2127–2135.
- (9) Green, K. D., Biswas, T., Chang, C., Wu, R., Chen, W., Janes, B. K., Chalupska, D., Gornicki, P., Hanna, P. C., Tsodikov, O. V., Joachimiak, A., and Garneau-Tsodikova, S. (2015) Biochemical and structural analysis of an Eis family aminoglycoside acetyltransferase from *Bacillus anthracis*. *Biochemistry* 54, 3197–3206.

(10) Green, K. D., Pricer, R. E., Stewart, M. N., and Garneau-Tsodikova, S. (2015) Comparative study of Eis-like enzymes from pathogenic and nonpathogenic bacteria. *ACS Infect. Dis.* 1, 272–283.

(11) Houghton, J. L., Green, K. D., Pricer, R. E., Mayhoub, A. S., and Garneau-Tsodikova, S. (2013) Unexpected *N*-acetylation of capreomycin by mycobacterial Eis enzymes. *J. Antimicrob. Chemother.* 68, 800–805.

(12) Pricer, R. E., Houghton, J. L., Green, K. D., Mayhoub, A. S., and Garneau-Tsodikova, S. (2012) Biochemical and structural analysis of aminoglycoside acetyltransferase Eis from *Anabaena variabilis*. *Mol. Biosyst.* 8, 3305–3313.

(13) Tsodikov, O. V., Green, K. D., and Garneau-Tsodikova, S. (2014) A random sequential mechanism of aminoglycoside acetylation by *Mycobacterium tuberculosis* Eis protein. *PLoS One* 9, No. e92370.

(14) Tehrani, K., and Martin, N. I. (2018) Beta-lactam/beta-lactamase inhibitor combinations: an update. *MedChemComm* 9, 1439–1456.

(15) Green, K. D., Chen, W., and Garneau-Tsodikova, S. (2012) Identification and characterization of inhibitors of the aminoglycoside resistance acetyltransferase Eis from *Mycobacterium tuberculosis*. *ChemMedChem* 7, 73–77.

(16) Willby, M. J., Green, K. D., Gajadeera, C. S., Hou, C., Tsodikov, O. V., Posey, J. E., and Garneau-Tsodikova, S. (2016) Potent inhibitors of acetyltransferase Eis overcome kanamycin resistance in *Mycobacterium tuberculosis*. *ACS Chem. Biol.* 11, 1639–1646.

(17) Garzan, A., Willby, M. J., Green, K. D., Gajadeera, C. S., Hou, C., Tsodikov, O. V., Posey, J. E., and Garneau-Tsodikova, S. (2016) Sulfonamide-based inhibitors of aminoglycoside acetyltransferase Eis abolish resistance to kanamycin in *Mycobacterium tuberculosis*. *J. Med. Chem.* 59, 10619–10628.

(18) Garzan, A., Willby, M. J., Green, K. D., Tsodikov, O. V., Posey, J. E., and Garneau-Tsodikova, S. (2016) Discovery and optimization of two Eis inhibitor families as kanamycin adjuvants against drug-resistant *M. tuberculosis*. *ACS Med. Chem. Lett.* 7, 1219–1221.

(19) Garzan, A., Willby, M. J., Ngo, H. X., Gajadeera, C. S., Green, K. D., Holbrook, S. Y., Hou, C., Posey, J. E., Tsodikov, O. V., and Garneau-Tsodikova, S. (2017) Combating enhanced intracellular survival (Eis)-mediated kanamycin resistance of *Mycobacterium tuberculosis* by novel pyrrolo[1,5-*a*]pyrazine-based Eis inhibitors. *ACS Infect. Dis.* 3, 302–309.

(20) Ngo, H. X., Green, K. D., Gajadeera, C. S., Willby, M. J., Holbrook, S. Y. L., Hou, C., Garzan, A., Mayhoub, A. S., Posey, J. E., Tsodikov, O. V., and Garneau-Tsodikova, S. (2018) Potent 1,2,4-triazino[5,6*b*]indole-3-thioether inhibitors of the kanamycin resistance enzyme Eis from *Mycobacterium tuberculosis*. *ACS Infect. Dis.* 4, 1030–1040.

(21) Green, K. D., Punetha, A., Hou, C., Garneau-Tsodikova, S., and Tsodikov, O. V. (2019) Probing the robustness of inhibitors of tuberculosis aminoglycoside resistance enzyme Eis by mutagenesis. *ACS Infect. Dis.* 5, 1772–1778.

(22) Zhang, J. H., Chung, T. D., and Oldenburg, K. R. (1999) A simple statistical parameter for use in revaluation and validation of high throughput screening assays. *J. Biomol. Screening* 4, 67–73.

(23) Tsodikov, O. V., Record, M. T., Jr., and Sergeev, Y. V. (2002) Novel computer program for fast exact calculation of accessible and molecular surface areas and average surface curvature. *J. Comput. Chem.* 23, 600–609.